Wiley
Advances in Condensed Matter Physics
Volume 2025, Article ID 8778603, 9 pages
https://doi.org/10.1155/acmp/8778603

WILEY

Research Article

Electronic Structure and Electrical Conductivity of $Ge_2Sb_2Te_5$ Heterostructures With Varying Stacking Configurations

Tomi Ketolainen and Janne Kalikka

Computational Physics Laboratory, Tampere University, P.O. Box 600, Tampere, FI-33014, Finland

Correspondence should be addressed to Tomi Ketolainen; tomi.ketolainen@tuni.fi

Received 22 May 2025; Revised 5 November 2025; Accepted 12 November 2025

Academic Editor: Sefer Bora Lisesivdin

Phase change materials (PCMs) are an important group of materials with distinct solid phases. In this group, $Ge_2Sb_2Te_5$ (GST) is a promising compound with many technological applications. GST can be grown into a heterostructure where the phase change is spatially confined, resulting in improved efficiency. In the present work, the electronic properties and electrical conductivity of GST heterostructures with various stacking configurations are studied using density functional calculations. Geometry optimization calculations show the importance of the van der Waals (vdW) correction that results in a decrease of the out-of-plane lattice parameter. Band structure calculations show metallic or semimetallic character for some configurations, whereas the others are semiconductors with bandgaps below 1 eV near the Γ point. The in-plane electrical conductivity is higher than the out-of-plane one, with differences between the configurations at most three- to fourfold, indicating they all belong to the same phase. The Te atoms are negatively charged, while the Ge and Sb atoms have positive charges. There is no significant charge transfer between the blocks separated by vdW gaps although visible electron accumulation occurs within the gaps. The observed stacking-dependent changes can possibly be applied to the design of interfacial PCMs with new properties and functionalities.

1. Introduction

The possibility of switching between the amorphous and crystalline phases by employing an electrical or optical pulse is an important property of chalcogenide phase change materials (PCMs) [1]. In this group of materials, $Ge_2Sb_2Te_5$ (GST) has become a promising PCM for various applications [2]. These PCMs can be switched with an external electrical or optical pulse between states with significant differences in their electrical resistivity and optical reflectivity, a property that can be utilized, for example, in nonvolatile memory and high-density optical recording devices, and optical switches [3–8]. Moreover, these phase transitions are reversible and occur on a timescale of tens of nanoseconds, which allows for fabricating memory devices with better performance than other current data storage systems.

The actual transitions between the amorphous and crystalline phases in GST are caused by Joule heating by an electrical or optical pulse [1]. Previous density functional calculations for crystallization of GST indicate that the crystallization process is complicated, comprising reorientation of rings with different atom types and changes in cavities [9–11]. The crystallization process can also induce some localized states that can affect the electronic properties of GST materials remarkably [12]. Furthermore, major challenges in GST materials are related, for example, to the resistance drift and stability. According to prior experimental and computational studies, the properties of chalcogenide PCMs can be improved significantly by doping them with various atoms [8, 13, 14].

In recent years, interfacial PCMs have turned out to be promising materials with a lot of technological potential [15, 16]. Conventional interfacial PCMs consist of well-ordered atomic planes or blocks bound by weak van der Waals (vdW) interactions [17, 18]. Compared with traditional PCMs, memory devices based on interfacial PCMs have lower switching energies, faster switching speeds, and enhanced performance regarding the number of write-erase cycles [15]. However, the precise atomic structures and switching mechanism of interfacial PCMs are not well known although a few possible mechanisms for explaining the electrical conductivity changes in interfacial PCMs have been proposed [19–23].

Previous experimental investigations indicate that the phase transitions in interfacial PCMs occur without melting, yet resulting in a significant change in the resistivity [15]. In this work, we carry out density functional calculations for GST heterostructures that are common interfacial PCMs. In particular, we study the effect of the stacking order on the electronic properties and electrical conductivity of hexagonal GST heterostructures. First, the crystal structures of GST heterostructures with six different stacking configurations are optimized. Next, we determine the electronic band structures for all the heterostructures of the present work. Thereafter, we compute the electrical conductivity for the heterostructures using the Boltzmann transport equation method within the constant relaxation time approximation. Our density functional calculations show that the stacking order affects both the structural properties and electrical conductivity of interfacial GST heterostructures.

The computational methodology is presented in Section 2. The optimized structures, lattice parameters, as well as the results from total energy, free energy, electrical conductivity, band structure, and charge transfer calculations are reported in Section 3. Finally, the results of the present work are summarized in Section 4.

2. Computational Methods

The electronic structure calculations of GST heterostructures are carried out using the Vienna *Ab initio* Simulation Package (VASP) based on density functional theory (DFT) and the projector augmented-wave method [24, 25]. We use both the PBE [26] and HSE06 [27] exchange-correlation functionals in this study. The PBE functional is used in the geometry optimization, free energy, and lateral electron density difference calculations. The band structure, bandgap, electrical conductivity, and Bader charge calculations are carried out using both functionals. We set the kinetic energy cutoff to 300 eV and employ a Γ-centered $6\times6\times2$ grid for k-point sampling in the calculations with 18 atoms. Both the lattice vectors and the atoms in the computational unit cells for GST heterostructures are optimized before performing actual ground state calculations for them. In the relaxation calculations, a convergence threshold of 0.005 eV Å^{-1} for forces is used. Moreover, we apply the DFT-D3 vdW correction to all DFT calculations of this work [28].

We calculate electrical conductivity for GST heterostructures with different layer orders with the BoltzTraP2 software package [29]. The BoltzTraP2 package uses the linearized Boltzmann transport equation for computing the transport coefficients, such as electrical conductivity. We also utilize information about the derivatives of electronic bands in the electrical conductivity calculations. The central quantity in Boltzmann transport calculations is the transport distribution function that can be written as [29]

$$\sigma_d(\varepsilon, T) = \int \sum_b \mathbf{v}_{b,\mathbf{k}} \otimes \mathbf{v}_{b,\mathbf{k}} \tau_{b,\mathbf{k}} \delta\left(\varepsilon - \varepsilon_{b,\mathbf{k}}\right) \frac{\mathrm{d}\mathbf{k}}{8\pi^3}, \quad (1)$$

where ε is the energy, T is the temperature, $\mathbf{v}_{b,\mathbf{k}}$ is the electron group velocity, and $\tau_{b,\mathbf{k}}$ is the relaxation time. In Equation (1), the symbols with subindices b and $\mathbf{k}$ mean that the values of the energies, group velocities, and relaxation times are determined for the electronic band b at a k-point $\mathbf{k}$. After computing the energy- and temperature-dependent transport distribution function, the electrical conductivity of the system can be determined. The electrical conductivity at a chemical potential μ and temperature T is given by Madsen et al. [29]:

$$\sigma(\mu, T) = q^2 \int \sigma_d(\varepsilon, T) \left(-\frac{\partial f(\varepsilon, \mu, T)}{\partial \varepsilon}\right) \mathrm{d}\varepsilon, \quad (2)$$

where ε denotes energy, q^2 is a term related to the volume of the computational unit cell, σ_d is the transport distribution function defined in Equation (1), and f is the Fermi distribution function.

As the relaxation time is complex due to phonon scattering and defects, we use the constant relaxation time approximation in all electrical conductivity calculations. In a previous computational study [30], the relaxation times of GST heterostructures with two stacking configurations have been calculated using the deformation potential theory. This study shows that the relaxation times of GST heterostructures are in the range of 10^{-13}–10^{-11} s with a dependence on the temperature. The GST has an electrical contrast of 2–3 orders of magnitude between the conductive and nonconductive states so it should be possible to distinguish those using the constant relaxation time approximation. In this work, the electrical conductivities of GST materials are expressed as σ/τ, where σ is the conductivity calculated using Equation (2) and τ is the constant relaxation time of the system. We compute the electrical conductivities at a temperature of 300 K. Furthermore, the free energy is calculated for all GST heterostructures with Phonopy 2.21 (for details of these calculations, see Ref. [31]). The superlattice structures are multiplied laterally to form 3×3 grids, and the resulting 162-atom structures are optimized with VASP using a plane-wave cutoff energy of 500 eV, self-consistent field cutoff energy of 10^{-8} eV, and maximum force cutoff of 0.002 eV Å^{-1}. A k-point mesh of $32\times32\times32$ sampling points is used within phonopy. We also use the Bader decomposition method to calculate charges of the Ge, Sb, and Te atoms in the unit cells of two GST heterostructures [32].

3. Results and Discussion

3.1. Total Energies and Lattice Parameters. The atomic structures of the six investigated GST heterostructures with different stacking configurations are presented in Figure 1. We consider the conventional Ferro, Petrov, Invpetrov, and Kooi structures [33–35] as well as the GA-opt and GA-switchable structures [36] that have been found using a genetic algorithm. We perform full relaxation for the six GST heterostructures. The total energies of the ground state calculations and the lattice parameters for all heterostructures after the PBE relaxation calculations are listed in Table 1.

The relaxation calculations show that the GA-opt structure has the lowest total energy although the differences between the total energies of all investigated GST systems are relatively small as shown in Table 1. The order of GST heterostructures

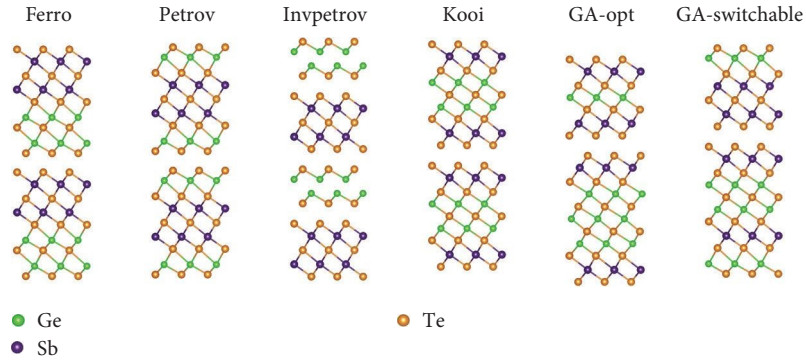

FIGURE 1: Atomic structures of GST heterostructures with the most common layer orderings. For each GST heterostructure, a side view of the $3 \times 3 \times 1$ supercell is displayed. The colors of the Ge, Sb, and Te atoms are as shown.

TABLE 1: Relative total energies and lattice parameters of GST heterostructures optimized using the PBE functional.

Stacking	E_{tot} (meV/atom)	a (Å)	c (Å)	$c/2$ (Å)
GA-opt	0.00	4.29	34.26	17.13
Kooi	1.27	4.30	34.31	17.15
Ferro	1.85	4.29	34.71	17.35
GA-switchable	6.40	4.27	34.70	17.35
Petrov	10.08	4.28	34.82	17.41
Invpetrov	14.58	4.23	36.01	18.01

Note: The GA-opt structure has the lowest total energy E_{tot} and that is set as zero. The in-plane and out-of-plane lattice parameters are denoted by a and c, respectively. The $c/2$ values are provided to ease the comparison with 9-atom structures commonly found in literature.

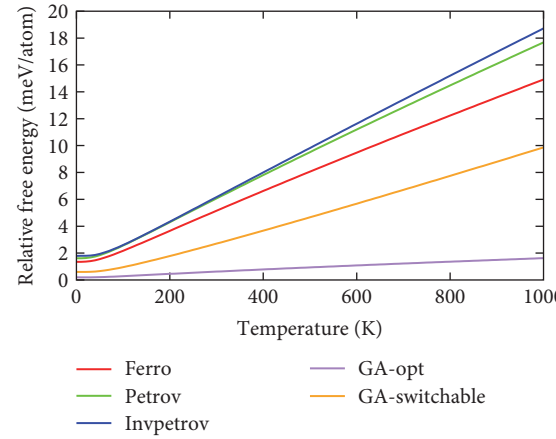

FIGURE 2: Relative free energies of GST heterostructures as a function of temperature. The free energies are calculated relative to the Kooi structure.

with respect to their total energies is very similar to that found in a previous computational study [36], the only difference being the order of Petrov and Invpetrov heterostructures. Furthermore, the order of GST heterostructures with respect to their relative total energies in the present study is in good agreement with other computational investigations of similar stacking configurations [37, 38]. On the other hand, the order of GST heterostructures and their relative total energies in the present work differ significantly from those obtained in another computational study where the largest relative total energy has been obtained for the Ferro configuration [33]. Here, the difference to present results can be related to different computational methods and settings used.

The in-plane lattice parameters (a) in Ref. [36] are close to the in-plane lattice parameters in the present work. Moreover, the in-plane lattice parameters calculated in a few other studies [33, 37, 38] are in good agreement with our results. In contrast, the out-of-plane lattice parameters (c) of Ref. [36] are larger than those obtained in our calculations. The former studies reported the out-of-plane lattice parameters (c) of the Kooi structure between 33.76 and 34.40 Å and the Ferro structure between 34.68 and 38.28 Å [33, 38]. Furthermore, in Refs. [33, 37, 38], the out-of-plane lattice parameters of 34.28–35.40 Å and 35.18–37.42 Å have been found for the Petrov and Invpetrov structures, respectively. The difference between the out-of-plane lattice parameters of our work and the previous computational studies most likely originates from the vdW correction, which is applied to our calculations but which was not utilized in Refs. [33, 36, 37].

According to the optimization calculations, there is a correlation between the relative total energies and lattice parameters, which can be stated by examining their values in Table 1. The in-plane lattice parameter a seems to decrease when the relative total energy of the GST heterostructure increases. Similarly, an increase in the relative total energy results in an increase in the out-of-plane lattice parameter c.

We also consider the effect of temperature on the stability of GST heterostructures and calculate their relative free energies. The results from the free energy calculations are displayed in Figure 2. These calculations indicate a linear dependence of the free energy on the temperature at above 100 K. The lowest free energy is obtained for the Kooi structure. As shown in Figure 2, the relative free energy differences between the GST heterostructures become significantly larger when the temperature increases. The order of free energy curves in Figure 2 is similar to that found in previous free energy calculations for the same GST heterostructures [36], but without the crossings of the free energy curves found in Ref. [36]. In addition, the relative free energy values of this work at high temperatures are four- to fivefold compared with those obtained in the former

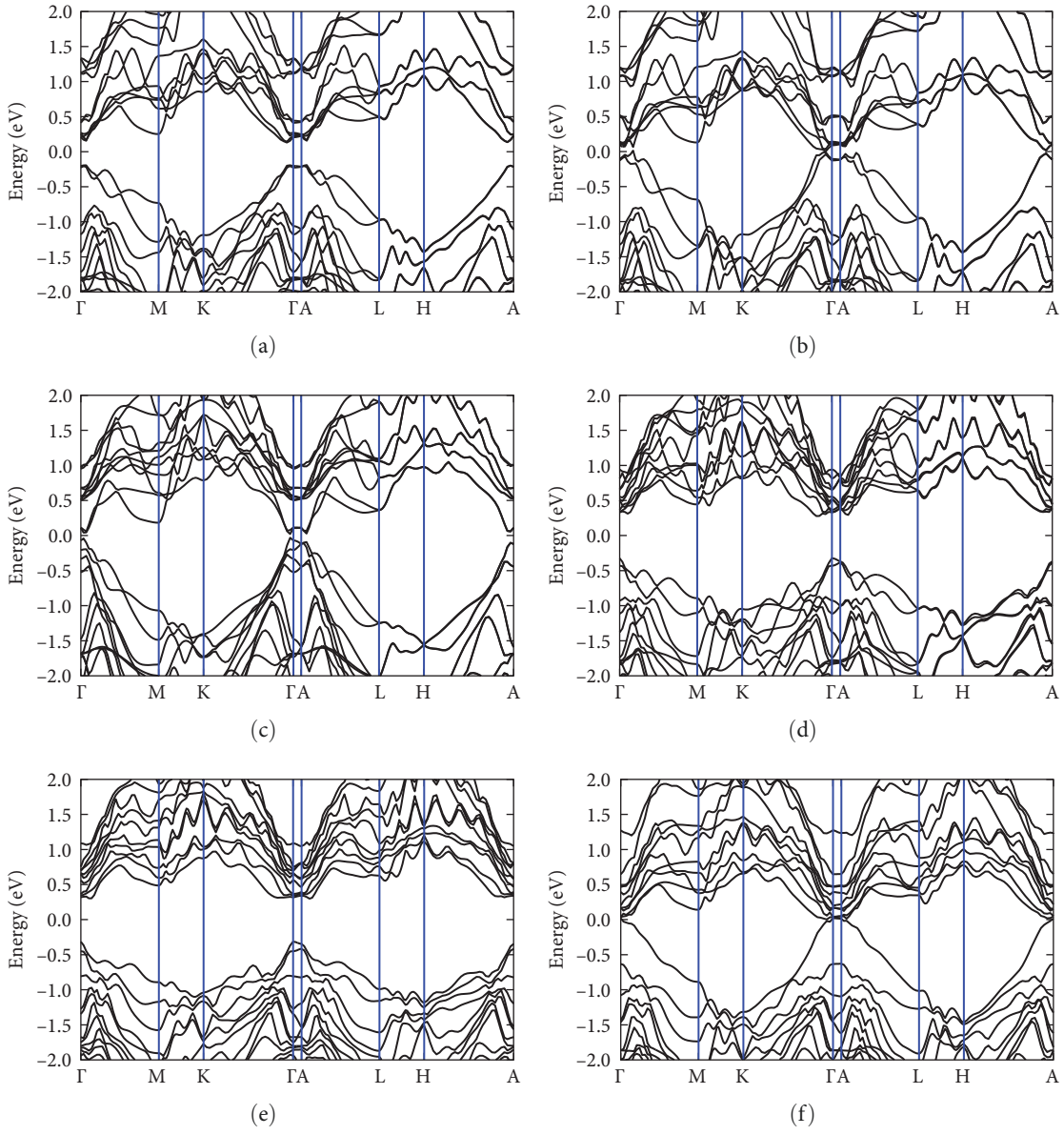

Figure 3: Band structures calculated using the HSE06 functional for (a) the Ferro, (b) Petrov, (c) Invpetrov, (d) Kooi, (e) GA-opt, and (f) GA-switchable heterostructures. The zero energy corresponds to the Fermi level.

calculations. A plausible explanation for the different free energy values and different shapes of the free energy curves can be related to the vdW correction used in the present work but not used in Ref. [36].

3.2. Band Structures. The electronic band structures of all six GST heterostructures calculated using the HSE06 functional are displayed in Figure 3. The corresponding band structures calculated using the PBE functional are presented in Figure S1 in the supporting information section. In the band structure plots, the left part (Γ, M, and K points) of each plot shows the band structure in the lower part of the first Brillouin zone. Correspondingly, the right part of the band structure plots (A, L, and H points) presents the upper part of the first Brillouin zone.

The band structure calculations show that the Ferro, Kooi, and GA-opt heterostructures are semiconductors with bandgaps close to the Γ point. On the other hand, metallic or semimetallic band structures are obtained for the Petrov, Invpetrov, and GA-switchable heterostructures. The PBE band structures in Figure S1 are very similar to the HSE06 band structures in Figure 3. However, the HSE06 bands are shifted with respect to those of PBE calculations, which results in wider bandgaps in the HSE06 calculations as usually found in hybrid functional calculations. The bandgaps of semiconducting GST heterostructures are presented in Table 2. In this table, the indirect and direct bandgaps are presented for both the PBE and HSE06 calculations. The PBE bandgaps are between 0.26 and 0.39 eV, and the values of the HSE06 bandgaps are between 0.41 and

Table 2: Indirect (E_g^{indir}) and direct (E_g^{dir}) bandgaps of semiconducting GST heterostructures.

Stacking	PBE		HSE06	
	E_g^{indir} (eV)	E_g^{dir} (eV)	E_g^{indir} (eV)	E_g^{dir} (eV)
Ferro	0.26	0.39	0.41	0.41
Kooi	0.37	0.37	0.66	0.66
GA-opt	0.33	0.33	0.63	0.63

Note: The bandgaps are shown for PBE and HSE06 calculations.

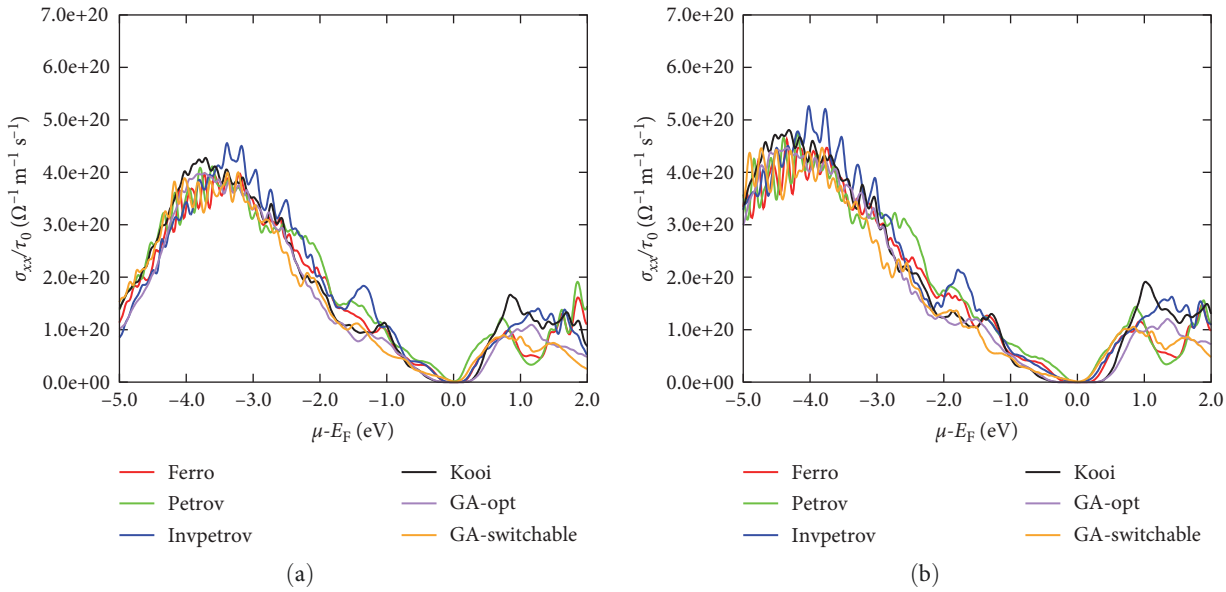

Figure 4: In-plane electrical conductivity calculated with (a) the PBE and (b) HSE06 functionals for different GST heterostructures.

0.66 eV. Therefore, all the bandgaps of the semiconducting heterostructures of the present work are close to 0.5 eV.

Previous computational studies of the band structures of GST heterostructures are mainly consistent with our band structure calculations [33, 37–40]. For the Ferro heterostructure, a metallic band structure has been found in Ref. [33], whereas another study [38] reported a semiconducting band structure. The Petrov and Invpetrov heterostructures have been found to have metallic band structures at least in two earlier studies [33, 37]. Instead, most earlier computational studies show that the Kooi heterostructure is a semiconductor with a bandgap close to the Γ point [33, 37–40].

3.3. Electrical Conductivity. The in-plane and out-of-plane electrical conductivity of GST heterostructures with different stacking orders is presented in Figures 4 and 5, respectively. In these figures, the in-plane (*xx* component) and out-of-plane (*zz* component) conductivities are computed as a function of the chemical potential using both the PBE and HSE06 functionals. Due to symmetry reasons, the *xx* and *yy* components of the in-plane conductivity turn out to be very similar. Thus, we show only the *xx* component of the in-plane electrical conductivity in the present work.

The results from the in-plane electrical conductivity calculations in Figure 4 show that the conductivity values are small in the Fermi energy region, which means that the investigated GST heterostructures are semiconducting. In addition, the values of the in-plane conductivity of all GST heterostructures are similar around the Fermi energy. On the other hand, the out-of-plane electrical conductivity curves in Figure 5 of the studied GST heterostructures are different from the in-plane results, and several peaks can be seen in all of them. Furthermore, the out-of-plane conductivity is clearly lower than the in-plane one, which results from the vdW gaps that lower the conductivity in this direction. The Kooi structure has a slightly higher out-of-plane electrical conductivity than the others. The differences between the out-of-plane conductivities of the GST heterostructures of the present work are at most three- to four-fold. In addition, the PBE results resemble the HSE06 ones. Shifts of the peaks further from the Fermi energy occur when the HSE06 functional is used instead of the PBE functional. Otherwise, the PBE and HSE06 results are consistent with each other. The relatively similar conductivities indicate that the switching does not happen between these structures but rather these are potential structures for the same interfacial PCM phase.

The in-plane conductivity curves in Figure 4 are mainly in good agreement with the respective calculations in a former study [41], where the values of the in-plane conductivity are of the same order of magnitude as those of the present work. Furthermore, the shapes of the in-plane conductivity curves are practically equivalent to ours. The out-of-plane electrical

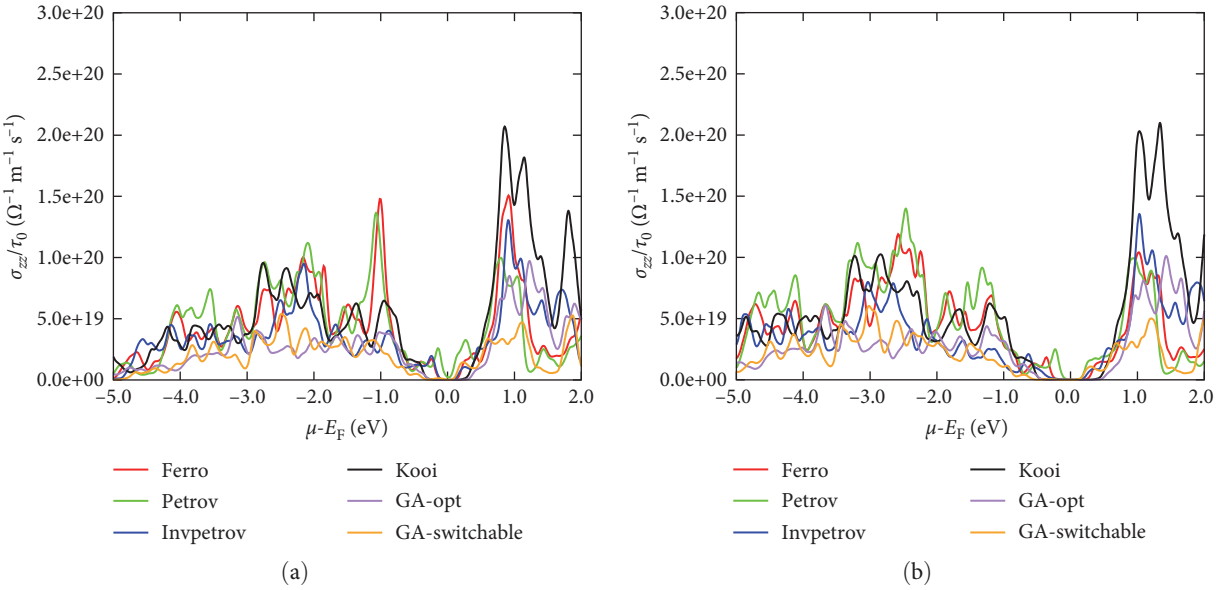

FIGURE 5: Out-of-plane electrical conductivity calculated with (a) the PBE and (b) HSE06 functionals for different GST heterostructures.

conductivity in Ref. [41], however, is clearly different from the results of the present work and does not have the sharp peaks seen in Figure 5. The parameters and computational settings of Ref. [41] differ from ours, which can explain the difference between the out-of-plane conductivities. In addition, a computational study by Tian et al. [30] reported a lower out-of-plane conductivity for the Kooi structure than for the Petrov structure. Hence, this result in the previous computational study is in disagreement with our conductivity calculations. On the other hand, the conductivity calculations have been carried out as a function of the charge carrier concentration and without scaling of the conductivity values with the inverse relaxation time τ^{-1} in Ref. [30], which may explain the higher out-of-plane conductivity of the Petrov stacking in that study.

3.4. Charge Analysis. We examine charge transfer by calculating Bader charges for individual atoms in the GST heterostructures. The charges calculated for the Kooi and GA-opt heterostructures using both the PBE and HSE06 functionals are listed in Table 3. The calculations show that the Ge and Sb atoms have positive charges, while the Te atoms are negatively charged. Moreover, the Te atoms are not as much negatively charged close to the vdW gap as they are farther away from them, that is, close to the center of a vdW block. The Bader charges of the Kooi and GA-opt heterostructures are similar, so the stacking sequence does not seem to affect the charge transfer between the atoms significantly. Furthermore, the charge transfer is found to be larger with the HSE06 functional than with PBE. The Bader charge studies indicate that the magnitude of the charge transfer is around 0.5 e in the Kooi and GA-opt heterostructures.

Since the charge transfer is smaller near the vdW gaps, it is also relevant to consider electron charge densities in different atomic layers of the GST heterostructure. We determine the lateral electron density difference that describes how the electron distribution changes when two vdW blocks form a complete heterostructure. The lateral electron density difference $\Delta\rho_\perp$ can be written as

$$\Delta\rho_\perp(z) = \rho_\perp^{\text{het}}(z) - \rho_\perp^{\text{lb}}(z) - \rho_\perp^{\text{ub}}(z)\ , \tag{3}$$

where $\rho_\perp^{\text{het}}$, $\rho_\perp^{\text{lb}}$, and $\rho_\perp^{\text{ub}}$ are the lateral electron densities of the whole structure, lower block, and upper block of the GST heterostructure, respectively.

The lateral electron density differences calculated at a distance z from the bottom of the unit cells for the Kooi and GA-opt heterostructures are similar as shown in Figure 6. In the case of both structures, the values of the $\Delta\rho_\perp$ vary as a function of the z-coordinate although the values near the center region of the vdW blocks are rather small. However, in the middle of the vdW gap, a noticeable peak in the lateral electron density difference is observed. This is likely due to the Te "lone pair" p electron density localizing in the gap. The Sb atom layers also become somewhat negatively charged. On the other hand, small positive charge accumulation is found close to the Te atom planes. Therefore, there is electron transfer from the Te atom layers to Ge and Sb ones when the two vdW blocks form a complete GST heterostructure. Furthermore, by integrating the lateral electron density difference curves over the z-coordinate regions where the lower and upper vdW blocks are located, we obtain an estimate for electron transfer between the two blocks in the GST heterostructure. The electron transfer from the lower block to the upper one in the Kooi structure is $\sim 4.8 \times 10^{-4}\, e$. In the GA-opt structure, the electron transfer from the lower block to the upper one is $\sim 9.7 \times 10^{-4}\, e$. These small charge values clearly show that there is no considerable charge transfer between the vdW blocks of the Kooi and GA-opt heterostructures. In a previous computational study, charge accumulation has been found at the Ge/Sb–graphene interface [42]. This result is in agreement with our electron density difference calculations.

Table 3: Bader charges Q_{Kooi} and $Q_{GA\text{-}opt}$ for the atoms in the Kooi and GA-opt heterostructures, respectively.

Atom	Q_{Kooi} (e)		Atom	$Q_{GA\text{-}opt}$ (e)	
	PBE	HSE06		PBE	HSE06
Te10	−0.37	−0.45	Te10	−0.36	−0.42
Sb4	0.61	0.73	Sb4	0.61	0.71
Te9	−0.48	−0.57	Te9	−0.48	−0.56
Ge4	0.46	0.56	Ge4	0.46	0.56
Te8	−0.46	−0.55	Te8	−0.49	−0.57
Ge3	0.46	0.55	Sb3	0.62	0.73
Te7	−0.48	−0.57	Te7	−0.37	−0.44
Sb3	0.62	0.73	Te6	−0.36	−0.43
Te6	−0.37	−0.44	Sb2	0.61	0.73
Te5	−0.36	−0.43	Te5	−0.48	−0.56
Sb2	0.60	0.71	Ge3	0.46	0.56
Te4	−0.46	−0.56	Te4	−0.47	−0.56
Ge2	0.46	0.56	Ge2	0.46	0.56
Te3	−0.47	−0.56	Te3	−0.46	−0.55
Ge1	0.46	0.55	Ge1	0.46	0.55
Te2	−0.47	−0.55	Te2	−0.48	−0.56
Sb1	0.61	0.72	Sb1	0.62	0.73
Te1	−0.37	−0.44	Te1	−0.37	−0.44

Note: The atoms in the table are listed according to the stacking sequences shown in Figure 1. The unit of the Bader charges is the elementary charge (e).

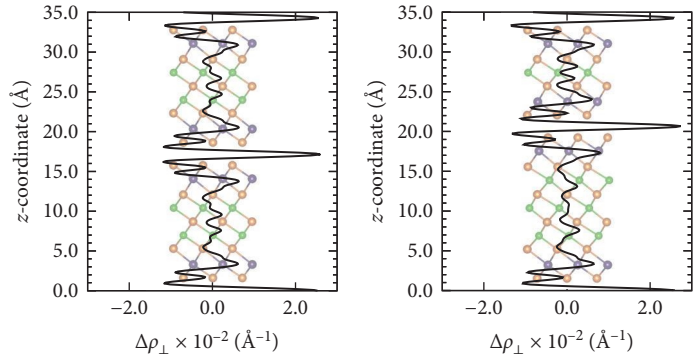

Figure 6: Lateral electron density differences of (a) the Kooi and (b) GA-opt heterostructures. Positive values denote electron accumulation. The atomic structures of the Kooi and GA-opt heterostructures are shown in both plots to guide the eye. The atoms are colored as shown in Figure 1.

4. Conclusion

We have studied the electronic properties and electrical conductivity of GST heterostructures with various stacking configurations. Moreover, we have considered the structural properties and thermodynamic stability of GST heterostructures. The GA-opt and Kooi stacking configurations are found to possess the lowest ground state energies, although the differences between the ground state energies of all studied stacking configurations are rather small. The band structure calculations reveal that the Petrov, Invpetrov, and GA-switchable stacking configurations result in semimetallic or metallic band structures. The Ferro, Kooi, and GA-opt stacking configurations have semiconducting band structures with bandgaps of ~0.5 eV. The bandgaps are usually located near the Γ point of the first Brillouin zone.

The Boltzmann transport equation calculations indicate that the in-plane conductivity is higher than the out-of-plane one, which is believed to be related to the vdW gaps between the blocks. The electrical conductivity becomes at most three- to fourfold when the stacking order of the GST heterostructure is changed. The results from the PBE and HSE06 calculations are qualitatively the same. The small relative differences in the conductivities of the six stacking orders indicate that the phase-change switching does not happen between any of them. The conductivity difference between the conductive and nonconductive phases is 2–3 orders of magnitude, so the studied stacking orders are all representative of the same, likely the conductive, phase of the interfacial PCM.

Furthermore, we have analyzed charge transfer in the GST heterostructures using two different approaches. The Te atoms have negative charges, whereas the other atoms (Ge and Sb) are

positively charged. There seems to be only a very small or even negligible charge transfer between the vdW blocks. However, electron charge is accumulated within the vdW gap region, likely due to Te "lone pair" *p* electrons. The results from electronic structure calculations show that the stacking configuration affects the band structures and electrical conductivity of GST heterostructures. Moreover, the findings of this work can give new insights into the development of new interfacial GST heterostructures that can be used to fabricate novel memory devices.

Data Availability Statement

The data that support the findings of this study are available from the corresponding author upon reasonable request.

Conflicts of Interest

The authors declare no conflicts of interest.

Funding

This study was funded by Research Council of Finland (Grants 332347, 336491, and 358167). Open access publishing facilitated by Tampereen yliopisto ja Tampereen ammattikorkeakoulu, as part of the Wiley - FinELib agreement.

Acknowledgments

We thank J. Akola for fruitful discussions. We acknowledge gratefully the computational resources provided by CSC - IT Center for Science (Project number 2004281). We thank the Research Council of Finland for financial support (Grants 332347, 336491, and 358167).

Supporting Information

Additional supporting information can be found online in the Supporting Information section. (*Supporting Information*) Description for the Supporting Information file. The electronic band structures calculated using the PBE functional for GST heterostructures are shown in Figure S1 in the Supporting Information file.

References

[1] P. Guo, A. M. Sarangan, and I. Agha, "A Review of Germanium-Antimony-Telluride Phase Change Materials for Non-Volatile Memories and Optical Modulators," *Applied Sciences* 9, no. 3 (2019): 530.

[2] S. R. Elliott, "Chalcogenide Phase-Change Materials: Past and Future," *International Journal of Applied Glass Science* 6, no. 1 (2015): 15–18.

[3] M. Wuttig and N. Yamada, "Phase-Change Materials for Rewriteable Data Storage," *Nature Materials* 6, no. 11 (2007): 824–832.

[4] S. Raoux and M. Wuttig, *Phase Change Materials: Science and Applications* (Springer, 2009).

[5] R. O. Jones, "Phase Change Memory Materials: Why Are Alloys of Ge, Sb, and Te the Materials of Choice?" *Solid State Sciences* 152 (2024): 107524.

[6] B.-S. Lee, J. R. Abelson, S. G. Bishop, D.-H. Kang, B.-K. Cheong, and K.-B. Kim, "Investigation of the Optical and Electronic Properties of $Ge_2Sb_2Te_5$ Phase Change Material in Its Amorphous, Cubic, and Hexagonal Phases," *Journal of Applied Physics* 97, no. 9 (2005): 093509.

[7] T. Kato and K. Tanaka, "Electronic Properties of Amorphous and Crystalline $Ge_2Sb_2Te_5$ Films," *Japanese Journal of Applied Physics* 44, no. 10 (2005): 7340–7344.

[8] N. Bala, B. Khan, K. Singh, P. Singh, A. P. Singh, and A. Thakur, "Recent Advances in Doped $Ge_2Sb_2Te_5$ Thin Film Based Phase Change Memories," *Materials Advances* 4, no. 3 (2023): 747–768.

[9] J. Akola and R. O. Jones, "Structural Phase Transitions on the Nanoscale: The Crucial Pattern in the Phase-Change Materials $Ge_2Sb_2Te_5$ and GeTe," *Physical Review B* 76, no. 23 (2007): 235201.

[10] J. Kalikka, J. Akola, J. Larrucea, and R. O. Jones, "Nucleus-Driven Crystallization of Amorphous $Ge_2Sb_2Te_5$: A Density Functional Study," *Physical Review B* 86, no. 14 (2012): 144113.

[11] J. Kalikka, J. Akola, and R. O. Jones, "Crystallization Processes in the Phase Change Material $Ge_2Sb_2Te_5$: Unbiased Density Functional/Molecular Dynamics Simulations," *Physical Review B* 94, no. 13 (2016): 134105.

[12] K. Konstantinou, F. C. Mocanu, and J. Akola, "Electron Localization in Recrystallized Models of the $Ge_2Sb_2Te_5$ Phase-Change Memory Material," *Physical Review B* 106, no. 18 (2022): 184103.

[13] X. Zhou, M. Xia, F. Rao, et al., "Understanding Phase-Change Behaviors of Carbon-Doped $Ge_2Sb_2Te_5$ for Phase-Change Memory Application," *ACS Applied Materials & Interfaces* 6, no. 16 (2014): 14207–14214.

[14] R. J. Appleton, Z. D. McClure, D. P. Adams, and A. Strachan, "Effects of Carbon Concentration on the Local Atomic Structure of Amorphous GST," *The Journal of Chemical Physics* 160, no. 17 (2024): 174702.

[15] R. E. Simpson, P. Fons, A. V. Kolobov, et al., "Interfacial Phase-Change Memory," *Nature Nanotechnology* 6, no. 8 (2011): 501–505.

[16] C. Yoo, J. W. Jeon, B. Park, et al., "A Review of Advances in Deposition Methods and Material Properties of Superlattice Phase-Change Memory," *ACS Applied Electronic Materials* 5, no. 11 (2023): 5794–5808.

[17] J. Tominaga, "The Design and Application on Interfacial Phase-Change Memory," *Physica Status Solidi (RRL): Rapid Research Letters* 13, no. 4 (2019): 1800539.

[18] R. Wang, R. Calarco, F. Arciprete, and V. Bragaglia, "Epitaxial Growth of GeTe/Sb_2Te_3 Superlattices," *Materials Science in Semiconductor Processing* 137 (2022): 106244.

[19] A. V. Kolobov, P. Fons, Y. Saito, and J. Tominaga, "Atomic Reconfiguration of Van der Waals Gaps as the Key to Switching in GeTe/Sb_2Te_3 Superlattices," *ACS Omega* 2, no. 9 (2017): 6223–6232.

[20] K. L. Okabe, A. Sood, E. Yalon, et al., "Understanding the Switching Mechanism of Interfacial Phase Change Memory," *Journal of Applied Physics* 125, no. 18 (2019): 184501.

[21] P. Fons, A. V. Kolobov, and Y. Saito, "Electric Fields and Interfacial Phase-Change Memory Structures," *Physica Status Solidi (RRL): Rapid Research Letters* 15, no. 3 (2021): 2000412.

[22] D. Térébénec, N. Castellani, N. Bernier, et al., "Improvement of Phase-Change Memory Performance by Means of GeTe/Sb_2Te_3 Superlattices," *Physica Status Solidi (RRL): Rapid Research Letters* 15, no. 3 (2021): 2000538.

[23] B. Liu, K. Li, J. Zhou, and Z. Sun, "Reversible Crystalline-Crystalline Transitions in Chalcogenide Phase-Change Materials," *Advanced Functional Materials* 34, no. 44 (2024): 2407239.

[24] G. Kresse and J. Furthmüller, "Efficient Iterative Schemes for Ab *Initio* Total-Energy Calculations Using a Plane-Wave Basis Set," *Physical Review B* 54, no. 16 (1996): 11169–11186.

[25] G. Kresse and D. Joubert, "From Ultrasoft Pseudopotentials to the Projector Augmented-Wave Method," *Physical Review B* 59, no. 3 (1999): 1758–1775.

[26] J. P. Perdew, K. Burke, and M. Ernzerhof, "Generalized Gradient Approximation Made Simple," *Physical Review Letters* 77, no. 18 (1996): 3865–3868.

[27] A. V. Krukau, O. A. Vydrov, A. F. Izmaylov, and G. E. Scuseria, "Influence of the Exchange Screening Parameter on the Performance of Screened Hybrid Functionals," *The Journal of Chemical Physics* 125, no. 22 (2006): 224106.

[28] S. Grimme, J. Antony, S. Ehrlich, and H. Krieg, "A Consistent and Accurate *Ab Initio* Parametrization of Density Functional Dispersion Correction (DFT-D) for the 94 Elements H-Pu," *The Journal of Chemical Physics* 132, no. 15 (2010): 154104.

[29] G. K. H. Madsen, J. Carrete, and M. J. Verstraete, "BoltzTraP2, a Program for Interpolating Band Structures and Calculating Semi-Classical Transport Coefficients," *Computer Physics Communications* 231 (2018): 140–145.

[30] J. Tian, W. Ma, P. Boulet, and M.-C. Record, "Electronic and Transport Properties of Strained and Unstrained $Ge_2Sb_2Te_5$: A DFT Investigation," *Materials* 16, no. 14 (2023): 5015.

[31] A. Togo, "First-Principles Phonon Calculations With Phonopy and Phono3py," *Journal of the Physical Society of Japan* 92, no. 1 (2023): 012001.

[32] G. Henkelman, A. Arnaldsson, and H. Jónsson, "A Fast and Robust Algorithm for Bader Decomposition of Charge Density," *Computational Materials Science* 36, no. 3 (2006): 354–360.

[33] J. Tominaga, A. V. Kolobov, P. Fons, T. Nakano, and S. Murakami, "Ferroelectric Order Control of the Dirac-Semimetal Phase in GeTe-Sb_2Te_3 Superlattices," *Advanced Materials Interfaces* 1, no. 1 (2014): 1300027.

[34] I. I. Petrov, R. M. Imamov, and Z. G. Pinsker, "Electron-Diffraction Determination of the Structures of $Ge_2Sb_2Te_5$ and $GeSb_4Te_7$," *Soviet Physics Crystallography* 13, no. 3 (1968): 339–342.

[35] B. J. Kooi and J. M. De Hosson, "Electron Diffraction and High-Resolution Transmission Electron Microscopy of the High Temperature Crystal Structures of $Ge_xSb_2Te_{3+x}$ (x = 1,2,3) Phase Change Material," *Journal of Applied Physics* 92, no. 7 (2002): 3584–3590.

[36] J. Kalikka, X. Zhou, J. Behera, G. Nannicini, and R. E. Simpson, "Evolutionary Design of Interfacial Phase Change Van der Waals Heterostructures," *Nanoscale* 8, no. 42 (2016): 18212–18220.

[37] W. Ibarra-Hernández and J.-Y. Raty, "*Ab Initio* Density Functional Theory Study of the Electronic, Dynamic, and Thermoelectric Properties of the Crystalline Pseudobinary Chalcogenide $(GeTe)_x/(Sb_2Te_3)$ (x = 1, 2, 3)," *Physical Review B* 97, no. 24 (2018): 245205.

[38] B. Sklénard, F. Triozon, C. Sabbione, et al., "Electronic and Thermal Properties of GeTe/Sb_2Te_3 Superlattices by *Ab Initio* Approach: Impact of Van der Waals Gaps on Vertical Lattice Thermal Conductivity," *Applied Physics Letters* 119, no. 20 (2021): 201911.

[39] J. Singh, G. Singh, A. Kaura, and S. K. Tripathi, "Electronic and Thermoelectric Properties of Layered Sn- and Pb-Doped $Ge_2Sb_2Te_5$ Alloys Using First Principle Calculations," *Journal of Electronic Materials* 45, no. 6 (2016): 2950–2956.

[40] Y. Huang, J. Zhou, L. Peng, K. Li, S. R. Elliott, and Z. Sun, "Antibonding-Induced Anomalous Temperature Dependence of the Band Gap in Crystalline $Ge_2Sb_2Te_5$," *The Journal of Physical Chemistry C* 125, no. 35 (2021): 19537–19543.

[41] J. Miao, P. Wang, P. Zhou, et al., "Remarkable Anisotropy in Rhombohedral $Ge_2Sb_2Te_5$ Compound: A Promising Thermoelectric Material With Multiple Conduction Bands and Acoustic-Optical Branches Coupling," *Journal of Alloys and Compounds* 900 (2022): 163471.

[42] S. Kulju, J. Akola, D. Prendergast, and R. O. Jones, "Tuning Electronic Properties of Graphene Heterostructures by Amorphous-to-Crystalline Phase Transitions," *Physical Review B* 93, no. 19 (2016): 195443.